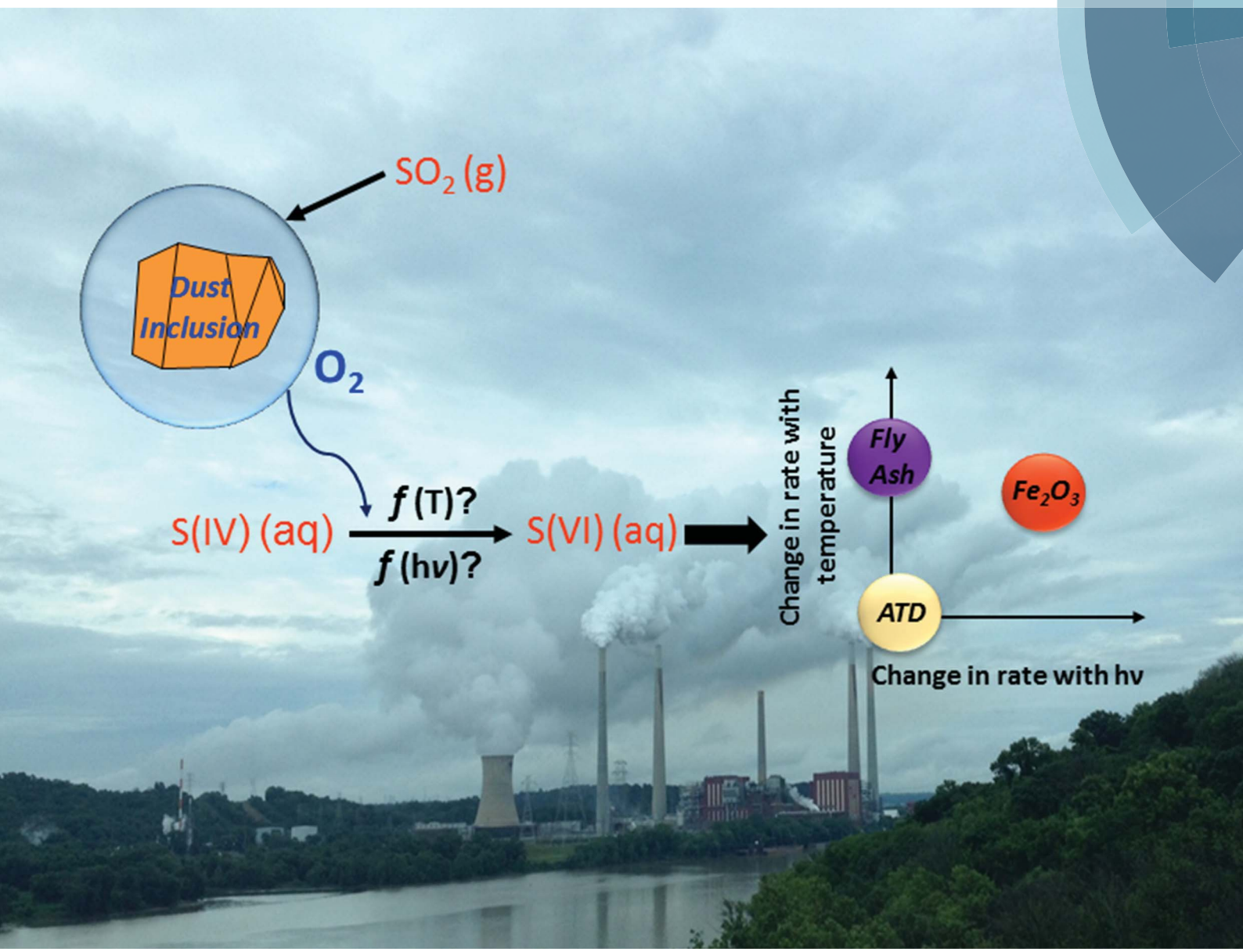
Volume 18 | Number 12 | December 2016 | Pages 1471–1574

Environmental Science
Processes & Impacts

rsc.li/process-impacts



ISSN 2050-7887

ROYAL SOCIETY OF CHEMISTRY

PAPER
Vicki H. Grassian *et al.*
Sulfate formation catalyzed by coal fly ash, mineral dust and iron(III) oxide: variable influence of temperature and light

175 YEARS

Environmental Science
Processes & Impacts

PAPER

View Article Online
View Journal | View Issue

Open Access Article. Published on 13 October 2016. Downloaded on 3/28/2024 8:14:22 PM.
This article is licensed under a Creative Commons Attribution 3.0 Unported Licence.

Cite this: *Environ. Sci.: Processes Impacts*, 2016, **18**, 1484

Sulfate formation catalyzed by coal fly ash, mineral dust and iron(III) oxide: variable influence of temperature and light†

Aruni Gankanda,[a] Ellen M. Coddens,[b] Yaping Zhang,[b] David M. Cwiertny[c] and Vicki H. Grassian*[bd]

Recent atmospheric field and modeling studies have highlighted a lack of understanding of the processes responsible for high levels of sulfate aerosol in the atmosphere, ultimately arising from a dearth of experimental data on such processes. Here we investigated the effect of temperature and simulated solar radiation on the catalytic oxidation of S(IV) to S(VI) (*i.e.*, sulfite to sulfate) in aqueous suspensions of several metal-containing, atmospherically relevant particles including coal fly ash (FA), Arizona test dust (ATD) and an iron oxide (γ-Fe_2O_3). The effect of temperature and light on S(IV) oxidation was found to be very different for these three samples. For example, in the presence of FA and γ-Fe_2O_3 the temporal evolution of dissolved Fe(II) (formed *via* reductive particle dissolution) correlated with S(IV) oxidation. Accordingly, we propose that S(IV) oxidation in most of these systems initially occurs primarily at the particle surface (*i.e.*, a heterogeneous reaction pathway), although a solution-phase (*i.e.*, homogeneous) catalytic pathway also contributes over later timescales due to the formation and accumulation of dissolved Fe(III) (generated *via* oxidation of dissolved Fe(II) by O_2). It is likely that the homogeneous reaction pathway is operative at initial times in the presence of γ-Fe_2O_3 at 25 °C. In contrast, S(IV) oxidation in the presence of ATD appears to proceed entirely *via* a heterogeneous reaction, which notably does not lead to any iron dissolution. In fact, the greater overall rate of S(IV) loss in the presence of ATD compared to FA and γ-Fe_2O_3 suggests that other factors, including greater adsorption of sulfite, transition metal ion (TMI) catalysis by other metal ions (*e.g.*, Ti), or different species of iron in ATD, play a role. Overall these studies suggest that the rate, extent and products of atmospheric S(IV) oxidation can be highly variable and dependent upon the nature of aerosol sources and ambient conditions (*e.g.*, temperature and irradiance). Ultimately, such complexity precludes simple, broadly generalized schemes for this reaction when modeling atmospheric processes involving diverse components of different mineral dust aerosol as well as other metal-containing aerosol.

Received 26th July 2016
Accepted 13th October 2016

DOI: 10.1039/c6em00430j

rsc.li/process-impacts

Environmental impact

Recent modeling studies to predict observed high levels of sulfate aerosol have been unsuccessful due to the lack of experimental data and poor understanding of the processes contributing to sulfate formation and the role of metal-containing particles. In this work, we have shown, for the first time, the varying effects of temperature and light on the catalytic oxidation of S(IV) to S(VI) in the presence of metal-containing, atmospherically relevant particles. Results of this study show that simple, broadly generalized schemes for S(IV) oxidation are insufficient when modeling atmospheric processes involving components of metal-containing and mineral dust aerosols due to the complex dependence on aerosol mineralogy and physicochemical properties.

Introduction

Sulfate aerosol in the atmosphere has a strong impact on climate due to their effect on direct radiative forcing and their ability to act as cloud condensation nuclei (CCN).[1–4] Anthropogenic SO_2 emitted by industrial activities (*e.g.*, fossil fuel burning) is the main precursor of sulfate in submicrometer particles.[1] It has been estimated that approximately 50% of global atmospheric SO_2 is ultimately oxidized to sulfate.[2] Understanding atmospheric sulfate formation pathways has

[a]*Department of Chemistry, University of Iowa, Iowa City, Iowa 52242, USA*
[b]*Department of Chemistry and Biochemistry, University of California San Diego, La Jolla, California 92093, USA. E-mail: vhgrassian@ucsd.edu*
[c]*Department of Civil and Environmental Engineering, University of Iowa, Iowa City, Iowa 52242, USA*
[d]*Departments of Nanoengineering and Scripps Institution of Oceanography, University of California San Diego, La Jolla, California 92093, USA*

† Electronic supplementary information (ESI) available. See DOI: 10.1039/c6em00430j

This journal is © The Royal Society of Chemistry 2016

Open Access Article. Published on 13 October 2016. Downloaded on 3/28/2024 8:14:22 PM.
This article is licensed under a Creative Commons Attribution 3.0 Unported Licence.

recently attracted a considerable amount of attention due to very high sulfate levels observed in severe haze conditions in China that cannot be explained using current atmospheric mechanisms and models.[5–11] Some of the recent studies suggest that the magnitude of this discrepancy can be reduced by incorporating catalyzed pathways for sulfate formation reactions involving mineral dust and other metal-containing aerosol in atmospheric models.[5,6]

Sulfur dioxide oxidation by molecular oxygen in the presence of transition metal ion (TMI) catalysts is an important S(IV) oxidation pathway in cloud/fog water,[12,13] estimated to contribute 9–17% of global sulfate production.[14] Fe(III) and Mn(II) are the most studied TMIs for aqueous phase S(IV) oxidation.[12,14] Recent studies suggest that this TMI catalyzed oxidation pathway is more important in winter relative to summer due to the lower atmospheric oxidation capacity because of weaker sunlight.[6,14] Unfortunately, this aqueous phase sulfur dioxide oxidation pathway has been excluded from most atmospheric chemistry models. This is mainly due to the uncertainties and limitations in the availability of chemical and kinetic data relevant to real atmospheric conditions for different meteorological and climate regimes and a lack of understanding of these processes as a function of important variables including temperature, pH and solar light.[6,14]

Specifically for iron-containing aerosol particles, ferric iron (Fe(III)) can drive sulfate formation from HSO_3^- either by a homogeneous (*i.e.*, solution phase) or heterogeneous (*i.e.*, at the solid–water interface) catalytic pathway, according to reactions (1)–(5).[15] For homogeneous catalysis, Fe(III) in mineral particles must first dissolve into the aqueous medium, where it then reacts with S(IV) ions to form sulfite radical. In the heterogeneous catalytic pathway, S(IV) species are first adsorbed on the particle surface, where they are then oxidized *via* an electron transfer reaction between surface or structural Fe(III) and adsorbed S(IV).[13] In the presence of O_2, this sulfite radical can be further oxidized to form sulfate ion *via* a series of chemical reactions. Fe(II) formed by the heterogeneous reaction pathway on particle surfaces will be more soluble than Fe(III). As a result, this Fe(II) can be released into the aqueous medium after its formation during the surface redox reaction (*i.e.*, reductive dissolution of iron), particularly at lower pH values.

$$Fe(III) + HSO_3^- \rightarrow Fe(II) + SO_3^- + H^+ \quad (1)$$

$$SO_3^- + O_2 \rightarrow SO_5^- \quad (2)$$

$$SO_5^- + Fe(II) + H^+ \rightarrow HSO_5^- + Fe(III) \quad (3)$$

$$HSO_5^- + Fe(II) \rightarrow SO_4^- + OH^- + Fe(III) \quad (4)$$

$$SO_4^- + Fe(II) \rightarrow SO_4^{2-} + Fe(III) \quad (5)$$

In the current study, we investigate the effect of low temperature and simulated solar radiation on S(IV) oxidation to sulfate in the presence of atmospherically relevant iron-containing mineral particles. These include a reference material for coal fly ash (FA), a pure iron(III) oxide phase (γ-Fe_2O_3) and Arizona test dust (ATD), which represents a proxy for mineral dust. Previous studies involving these samples have shown they contain iron-bearing solid phases that may be directly reactive toward adsorbed sulfate (*i.e.*, a heterogeneous catalytic pathway) and can also produce dissolved iron in aqueous solutions (*i.e.*, a homogeneous catalytic pathway) under certain conditions.[16–18] Our main focus here is to begin to develop an understanding as to the effect of different atmospherically relevant conditions, particularly, low temperature and solar radiation, on S(IV) oxidation by structural and leached iron from particles with different phases and mineralogy. Interestingly, we report highly variable effects of these conditions depending on the source material used in these studies, suggesting that there is a complex dependence of S(IV) oxidation on aerosol properties and their detailed physicochemical characteristics.

Materials and methods

Mineral and TMI containing aerosol samples

FA standard reference material (SRM 2690, National Institute of Standards and Technology), Arizona test dust (ISO 12103-1 A2 test dust, Powder Technology Inc.) and γ-Fe_2O_3 (Alfa Aesar) were used as received. Specific surface areas of solid samples were characterized using Quantachrome Nova 4200e BET surface area analyzer.

Simulated in-cloud aqueous phase S(IV) oxidation in the presence of atmospherically relevant particles

All S(IV) oxidation experiments were carried out in water-jacketed glass vessels containing an appropriate volume of S(IV) solution and mineral aerosol sample. In a typical experiment, a 2 mM (or 1.5 mM in low temperature experiments) aqueous S(IV) solution was prepared by dissolving Na_2SO_3 (Fisher) in Optima water (Fisher) at 25 °C or 15 °C as appropriate (pH $\sim$ 8.3). Then the pH of this solution was adjusted to pH = 5 using dilute HCl and NaOH. The final concentration of S(IV) in all the pH adjusted solutions was 1 $\pm$ 0.2 mM, where the decrease in S(IV) during pH adjustment resulted from elimination of gas-phase SO_2 by the reaction of HCl with Na_2SO_3 and stirring. A solid loading of 1 g L^{-1} was used in all experiments. All solutions were continuously stirred in the presence of atmospheric oxygen during the experiment to maintain a well-dispersed solid suspension.

Experiments were initiated by adding the solid samples into glass vessels containing 50 mL of 1 mM sulfite solution. Subsequently, 8 mL aliquots of the reaction mixture were periodically withdrawn over time and filtered with a 0.2 μM nylon filter (Xpertek). This filtered solution was immediately used to analyze for S(IV) concentration, dissolved Fe(II), and total dissolved iron (Fe(III) + Fe(II)), and also to measure pH. Experiments with FA and γ-Fe_2O_3 were carried out for 120 min and the reactions with ATD were carried out for 60 min. FA and samples were withdrawn at 20, 40, 60, 90 and 120 min time intervals. ATD samples were withdrawn at 10, 20, 30, 40 and 60 min time intervals. All results represent the average and standard error of three replicate experiments. Control experiments in the absence

Open Access Article. Published on 13 October 2016. Downloaded on 3/28/2024 8:14:22 PM. This article is licensed under a Creative Commons Attribution 3.0 Unported Licence.

of any particles were also conducted at 25 °C and 15 °C, as well as under simulated solar irradiation.

In order to determine the effect of simulated solar radiation on S(IV) oxidation, reaction mixtures at 25 °C were irradiated with a 150 W xenon arc lamp (Oriel Corp.). Light coming from the xenon arc lamp was filtered with a Pyrex filter before reaching the reaction mixture in all the photochemical experiments, resulting in wavelengths >300 nm incident to the reactor. All the experiments were conducted inside a dark room in order to avoid any reactions promoted by room light.

Analytical methods

The S(IV) concentrations were determined using the method described by Humphrey *et al.* using DTNB (5,5′-dithiobis-(2-nitro-benzoic acid)) as the colorimetric agent.[13,19] Fe(II) and total iron concentrations were determined with 1,10-phenanthroline as described in detail previously.[16,20]

ATR-FTIR spectroscopy

ATR-FTIR spectroscopy measurements of S(IV) oxidation were taken using a Thermo-Nicolet spectrometer equipped with an MCT/A detector. An evenly coated sample thin film (FA, γ-Fe_2O_3, ATD) was deposited onto a Ge crystal element in a horizontal ATR cell (Pike Technologies, Inc.). One mL of Optima water (Fisher) was pipetted onto the thin film and a background spectrum was collected. An aqueous solution of S(IV) was prepared by dissolving Na_2SO_3 (Fisher) in Optima water (Fisher) and the pH was adjusted to 5 using dilute HCl. After pipetting off the water, 1 mL of the aqueous S(IV) solution (50 mM for FA and γ-Fe_2O_3, 100 mM for ATD) was added to the surface. A glass slide was placed on the horizontal cell to prevent evaporation. A total of 200 scans were acquired for each spectrum and spectra were collected every 5 minutes for 3 hours.

Results

Characterization of FA, ATD and γ-Fe_2O_3

BET-measured specific surface areas of FA, ATD and γ-Fe_2O_3 were 3.8 ± 0.1, 4.2 ± 1.0 and 56 ± 1 $m^2\ g^{-1}$, respectively. The total iron content, iron speciation, and iron enrichment on the surface of FA and ATD particles used in the current study were previously characterized in detail by our group (Cwiertny *et al.* and Chen *et al.*) using acid digestion methods, Mossbauer spectroscopy, scanning electron microscopy coupled with energy dispersive X-ray spectroscopy (SEM/EDX) and X-ray photoelectron spectroscopy (XPS).[16–18] SEM/EDX provides information relating to the bulk material composition, whereas XPS provides information specific to the near-surface region of the mineral particles.

FA contains 3.57 ± 0.006 wt% iron, while iron content in ATD is 1.98 ± 0.08 wt%. Both FA and ATD contain a significant amount of iron associated with aluminosilicates.[17,18] However, in FA these aluminosilicates are dominantly in a glassy state formed *via* high temperature combustion followed by fast cooling.[18] In FA, iron speciation included 38% Fe(III) and 17% Fe(II) in aluminosilicate glasses, as well as 45% Fe(III) in oxides.[18] In ATD, Fe(III) exists both in crystalline aluminosilicates and oxides, whereas Fe(II) is present as Fe(II)-substituted aluminosilicate.[17,18] In comparing the surface-to-bulk concentration of Fe in ATD, the ratio of measured XPS to EDX response was greater than unity, indicates an enrichment of Fe on the ATD particle surface. In contrast, this ratio for other elements detected in ATD (Si, Al, Fe, Mg, Ca, K and Na) was equal to one, indicating that the surface composition reflects the elemental composition in the bulk of ATD particles.[16] A similar analysis was conducted for FA, where the ratio of XPS to EDX response for Si and Al were less than 1, indicating their enrichment in the bulk of FA particles.[18] For Fe, this ratio was equal to 1.4 ± 0.3, once again indicating a modest enrichment of iron on the surface of FA.[18] Also for FA, there was good agreement between the surface and bulk concentrations of Ca and K, while Mg and Na were also surface enriched.[18] According to the XRD pattern, γ-Fe_2O_3 is 100% crystalline iron(III) oxide.

Effect of temperature on S(IV) oxidation in the presence of FA, ATD and γ-Fe_2O_3

Changes in S(IV) concentration and the corresponding variation of total dissolved iron and Fe(II) over time in the presence of FA, γ-Fe_2O_3 and ATD particles are shown in Fig. 1a–c, respectively. The concentration of S(IV) in the solution decreased over time for all three aerosol samples. Analysis of the filtered reaction mixture carried out at 25 °C in the presence of all three aerosol samples with ATR-FTIR spectroscopy revealed that this S(IV) loss accompanies the formation of solution phase sulfate ions characterized by an infrared adsorption band near 1100 cm^{-1}. Representative results from ATR-FTIR analysis of filtrate from reacted ATD suspensions are shown in Fig. S1,† where the feature at 1100 cm^{-1} associated with sulfate clearly grows in over time. We note that results of control experiments conducted in the absence of aerosol materials (Fig. S2†) showed a smaller loss of S(IV) compared to the experiments conducted in the presence of mineral particles.

Additional *in situ* ATR-FTIR spectroscopic studies for the different samples as a function of time are shown in Fig. 2. It is important to note that these experiments were carried out under higher sulfite concentrations. The absorption band near 1100 cm^{-1}, corresponding to aqueous phase sulfate, is present for all three samples. As time progresses, the intensity of the sulfate feature increases indicating that the oxidation of S(IV) to S(VI) and subsequent formation of sulfate increases as a function of time.

Rates of S(IV) loss calculated assuming a linear relationship between time and S(IV) loss are summarized for all aerosol materials in Table 1. For FA (Fig. 1a) and γ-Fe_2O_3 (Fig. 1b), the rate of S(IV) loss decreased when the reaction temperature was lowered from 25 °C to 15 °C. Similarly, a corresponding decrease in the extent of iron dissolution was also observed with this lowering of temperature. Temperature also influenced the dissolved iron speciation for both FA and γ-Fe_2O_3. For example, at 25 °C, the fraction of dissolved Fe(II) increased relatively

 This journal is © The Royal Society of Chemistry 2016

Open Access Article. Published on 13 October 2016. Downloaded on 3/28/2024 8:14:22 PM.
This article is licensed under a Creative Commons Attribution 3.0 Unported Licence.

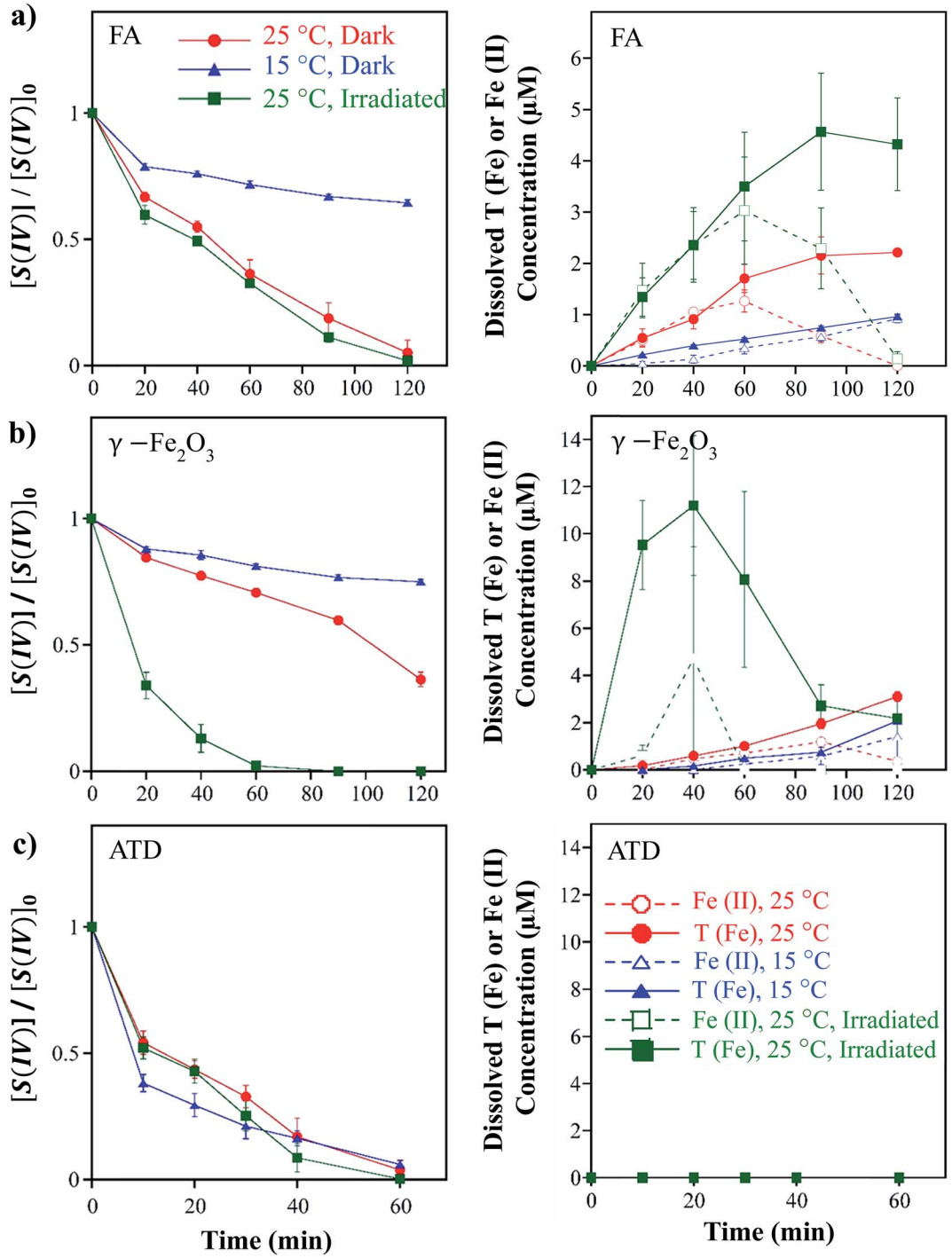


Fig. 1 Change in normalized S(IV) concentration and absolute dissolved Fe(II) and T(Fe) (total dissolved iron) concentrations with time in the presence of (a) FA, (b) γ-Fe_2O_3 and (c) ATD under different reaction conditions. In these figures, normalized S(IV) concentrations were obtained by taking the ratio of the S(IV) concentration at some time t ([S(IV)]) to the initial S(IV) concentration ($[S(IV)]_0$) of each experiment. Note the different time scale for ATD.

quickly over the first 20 to 40 min of reaction for both FA and γ-Fe_2O_3 and then decreased rather sharply over longer timescales until reaching zero (*i.e.*, all dissolved iron was Fe(III) after 120 min) (Fig. 3). In contrast at 15 °C in FA systems, the fraction of dissolved Fe(II) increased monotonically over time, until nearly all dissolved iron was ferrous iron (Fe(II)) after 120 minutes. For γ-Fe_2O_3, dissolved Fe(II) was only measurable after 20 min at 25 °C, after which Fe(II) concentrations steadily decreased for the remainder of the experiment. At 15 °C, Fe(II) formation was slower, only observed after 40 min and then achieving a maximum after 90 min before starting to decrease in a pattern similar to what was observed at 25 °C.

Open Access Article. Published on 13 October 2016. Downloaded on 3/28/2024 8:14:22 PM.
This article is licensed under a Creative Commons Attribution 3.0 Unported Licence.

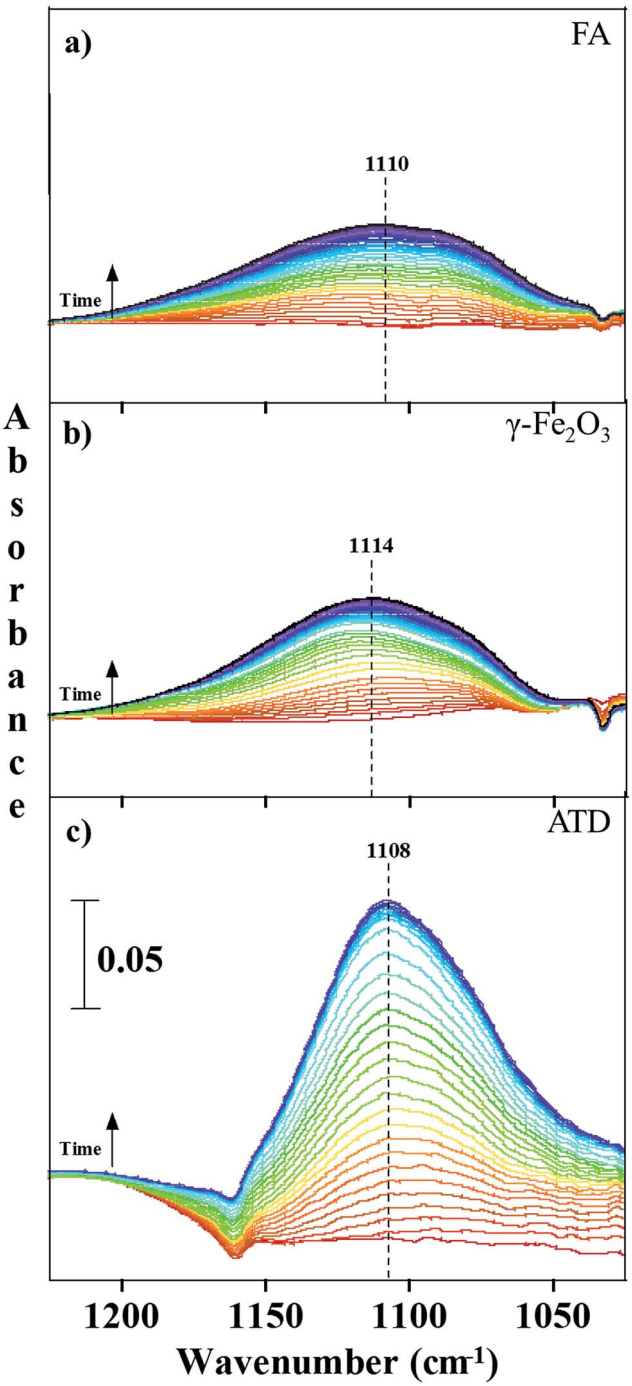


Fig. 2 ATR-FTIR spectra of S(IV) oxidation in the presence of FA, γ-Fe_2O_3, and ATD thin films on the ATR crystal. The infrared absorption bands near 1100 cm^{-1} correspond to solution phase sulfate. The spectra for FA and γ-Fe_2O_3 were collected using a 50 mM solution of sodium sulfite at pH 5. Because the ATD film on the ATR crystal was more difficult to stabilize, it was determined that the best spectra for ATD could be obtained at a higher concentration of 100 mM sodium sulfite at pH 5. The *y*-axis scale is the same for (a–c).

Table 1 Rate of S(IV) loss in the presence of FA, γ-Fe_2O_3 and ATD

	Rate $\times 10^{-3}$ (mM s^{-1})		
Reaction condition	FA	γ-Fe_2O_3	ATD
15 °C	3.2 ± 0.2	2.0 ± 0.1	17.1 ± 0.5
25 °C	8 ± 2	6.4 ± 0.5	15 ± 2
25 °C, irradiated	9 ± 2	13 ± 2	15.9 ± 0.8

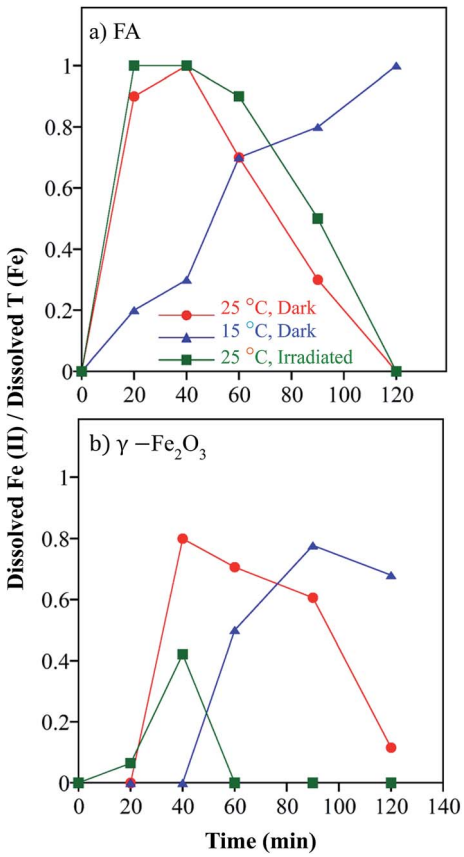


Fig. 3 The fraction of total dissolved Fe percent as Fe(II) as a function of time for (a) FA and (b) γ-Fe_2O_3.

In contrast to the temperature dependent behavior observed for FA and γ-Fe_2O_3 dissolution, the rate and the magnitude of S(IV) loss in the presence of ATD was independent of temperature over the range considered (Fig. 1c), yielding statistically equivalent rates of S(IV) loss at 25 and 15 °C (Table 1). Notably, and also unlike FA and γ-Fe_2O_3, iron dissolution was not observed in the presence of ATD at either temperature despite the observation of sulfate formation *via* ATR-FTIR analysis (see Fig. S1†), indicating that S(IV) oxidation does indeed takes place in ATD systems.

Finally, Table 2 shows the variation of solution pH in the presence of different aerosol materials over the course of dissolution experiments. S(IV) oxidation in the presence of FA and γ-Fe_2O_3 acidified the reaction mixture, with a typical decrease in initial solution pH (pH = 5) between 1 and 1.5 pH units over 120 min reaction time. For ATD, on the other hand, initial solution pH increased roughly one pH unit over 60 min reaction time. These changes in pH were comparable across all temperatures (as well as other reaction conditions discussed hereafter).

This journal is © The Royal Society of Chemistry 2016

Open Access Article. Published on 13 October 2016. Downloaded on 3/28/2024 8:14:22 PM.
This article is licensed under a Creative Commons Attribution 3.0 Unported Licence.

Table 2 Initial and final pH of the reaction mixture in the presence of FA, γ-Fe_2O_3 and ATD and their comparison with control

	pH variation (initial − final)				
Reaction condition	FA (120 min)	γ-Fe_2O_3 (120 min)	Blank (120 min)	ATD (60 min)	Blank (60 min)
25 °C	5.0–4.0	5.1–3.5	5.1–4.5	5.1–6.1	5.1–4.6
15 °C	5.1–3.8	5.0–4.2	5.1–4.9	5.0–5.8	5.1–5.3
25 °C, irradiated	5.1–4.1	5.0–3.4	5.1–4.4	5.0–6.1	5.1–4.5

Effect of simulated solar radiation on S(IV) oxidation in the presence of FA, ATD and γ-Fe_2O_3

The effect of simulated solar radiation on S(IV) loss and soluble iron dissolution was investigated at 25 °C. As shown in Fig. 1, the influence of simulated solar radiation on S(IV) loss at 25 °C is different for FA, γ-Fe_2O_3 and ATD. For FA and ATD systems (Fig. 1a and c, respectively), S(IV) loss under irradiation was practically identical to the loss observed in dark experiments. In contrast, a much greater rate of S(IV) loss was measured in the presence of γ-Fe_2O_3, where a two-fold increase in S(IV) loss was measured in the light relative to dark suspensions, with S(IV) reaching concentrations below the method detection limit by 90 min.

The influence of light on the rate, extent and speciation of iron dissolution was also highly variable depending on the nature of the aerosol material. First, dissolved iron remained unmeasurable (*i.e.*, below detection limits) in irradiated ATD systems, as was also observed in dark systems at both temperatures considered. In the presence of FA, despite similar rates of S(IV) loss in light and dark systems, iron dissolution was significantly increased under irradiation (by roughly a factor of two), although the relative speciation of dissolved Fe(II) to Fe(III) was nearly identical in both systems (Fig. 3). Specifically, in both light and dark systems, an initially large fraction of Fe(II) gradually transitioned over time to exclusively Fe(III) in solution. For γ-Fe_2O_3, the two-fold increase in S(IV) loss coincided with a considerable increase in iron dissolution in irradiated systems. In the irradiated system, the overwhelming majority of the dissolved iron was Fe(III), with small amounts of Fe(II) only detected at 20 (~5% of total iron) and 40 min (~40% of total iron) sampling times. Thus, in irradiated γ-Fe_2O_3 systems, dissolved Fe(III) is the dominant form at all time scales, and present exclusively in solution over longer time intervals. Control experiments were conducted using pH = 5 Optima water under irradiation (in the absence of S(IV)) for the γ-Fe_2O_3 system. However, we did not detect any soluble iron, suggesting that iron dissolution is insignificant in the absence of sulfite, even in irradiated systems. This suggests that the observed iron dissolution in irradiated systems with γ-Fe_2O_3 is due to the presence of S(IV).

Discussion

S(IV) oxidation in FA and γ-Fe_2O_3 systems

For light and dark FA systems at 25 °C, the observation that Fe(II) and total Fe are equivalent at early timescales suggests that iron dissolution is most likely dominated by a reductively driven process. Further, the lack of measureable soluble Fe(III) also implies the dominance of a surface-mediated, heterogeneous catalytic pathway (Fig. 4) for S(IV) oxidation in FA systems at these conditions, at least at early times along the reaction coordinate. At longer timescales, where total iron concentration starts to exceeds Fe(II) concentration, dissolved Fe(III) starts to gradually accumulate in the aqueous phase. This increase in Fe(III) concentration may be due to three reasons; (i) air oxidation of Fe(II) in the solution phase and (ii) oxidation of Fe(II) to Fe(III) *via* the processes described earlier in reactions (3) through (5) (iii) increased proton promoted dissolution of Fe(III) due to decrease in pH (Table 2). Previous studies by Cwiertny *et al.* and Fu *et al.* also show that iron dissolution from mineral particles is enhanced with lowering of pH (form pH = 3 to 1) due to increased proton promoted dissolution.[16,20] Increased protonation of mineral particle surfaces weakens the critical Fe–O lattice bonds that enables the detachment of Fe cations from oxides into the solution.[20] Nevertheless, once sufficient dissolved iron is generated in solution, a homogeneous reaction pathway (Fig. 4) may be viable for S(IV) oxidation, especially at later times in FA systems. This is consistent with a previous study by Rani *et al.* focusing on S(IV) oxidation in the presence of atmospheric dust, which also suggested initial heterogeneous catalysis was followed by homogeneous catalysis at later times.[21,22]

For this heterogeneous reaction pathway, we note that because the stability constants for $FeSO_4^+$ and $FeSO_3^+$ are $10^{2.0}$ M^{-1} and $10^{8.8}$ M^{-1},[23] respectively, S(IV) is capable of displacing sulfate ions from surface coordination sites after their production. Therefore, adsorbed sulfate is not likely to inhibit the S(IV) oxidation reaction in FA (or other) systems.[13] This is also consistent with our observation of solution phase sulfate ions accumulating in these experimental systems over time *via* infrared spectroscopic analysis.

Regarding the influence of temperature and light on FA systems, the decrease in the rate of S(IV) loss and iron dissolution observed at 15 °C compared to 25 °C presumably reflects the slower reaction kinetics typical of most thermal dissolution processes at lower temperature. Further, for irradiated systems, the increased iron dissolution in the presence of FA without a significant change in S(IV) loss compared to dark systems at 25 °C may suggest that S(IV) loss is dominated by sorption rather

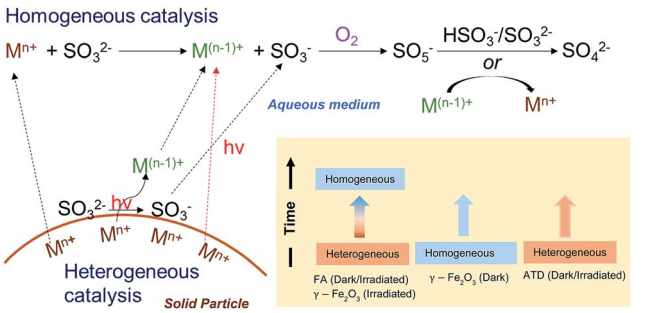


Fig. 4 Schematic of the mechanisms of S(IV) oxidation in the presence of mineral dust.

Open Access Article. Published on 13 October 2016. Downloaded on 3/28/2024 8:14:22 PM.
This article is licensed under a Creative Commons Attribution 3.0 Unported Licence.

than reaction, and that sorption primarily occurs on sites other than those iron sites involved in photoreductive dissolution.

For dark γ-Fe_2O_3 systems at 25 °C, a different primary mechanism for S(IV) oxidation is likely at play. Specifically, the majority of soluble iron observed at early timescales is Fe(III), and Fe(II) is only observed at later times. This suggests that the majority of the initial dissolution of γ-Fe_2O_3 is not reductively driven, but rather occurs by some other mode of dissolution (*e.g.*, proton or ligand promoted). Further, the observation of Fe(II) only at later times is most consistent with its production in aqueous solution, presumably *via* the homogeneous oxidation of S(IV) by soluble Fe(III). Although proton mediated dissolution of Fe(III) is another possible pathway, this is unlikely at initial times due to very low solubility of Fe(III) at higher pH.[20]

During irradiation of γ-Fe_2O_3 systems, S(IV) oxidation may be heterogeneous and photochemically driven. Specifically, light absorption by iron oxide particles can lead to the formation of electron (e^-)–hole (h^+) pairs. These electron–hole pairs can lead to one electron oxidation of adsorbed sulfite to $SO_3^{\bullet -}$ (or S(V)) as shown in reaction (6) and (7).[13]

$$\mathrm{Fe(III)} + \mathrm{S(IV)} \rightarrow \mathrm{Fe(II)} - \mathrm{S(IV)}_{\mathrm{surface}} \quad (6)$$

$$\mathrm{Fe(II)} - \mathrm{S(IV)} \xrightarrow{h\nu} \mathrm{S(V)}_{\mathrm{surface}} + \mathrm{Fe(II)}_{\mathrm{aq}} \quad (7)$$

Once on the surface, these S(V) species can react with a h^+ to produce S(VI) that is then released into the aqueous medium (reaction (8)).

$$\mathrm{S(V)}_{\mathrm{surface}} + h^+ \rightarrow \mathrm{S(VI)}_{\mathrm{aq}} \quad (8)$$

We speculate that this photoprocess may account for the considerably greater S(IV) loss observed with γ-Fe_2O_3 under irradiation. Due to the photo activity of γ-Fe_2O_3, in the presence of light and O_2, reactive oxygen species produced in this system, such as $OH^{\bullet}$, $O_2^{\bullet -}$, $HO_2^{\bullet}$ and H_2O_2, can also oxidize S(IV) to S(VI).[22] However, formation of these reactive oxygen species need some time and more favorable under acidic pH conditions. Therefore it is likely that the oxidation by reactive oxygen species are more favorable in later times where the pH of the reaction system is <4 (Table 2). H_2O_2 is the main S(IV) oxidant in the atmosphere for pH values below 5.[24] However, this is formed by secondary reactions of other reactive oxygen species, mainly by the self-reaction of $HO_2^{\bullet}$.[25] Therefore, in the γ-Fe_2O_3 system, reactions of H_2O_2 is possible in much later times compared to $OH^{\bullet}$, $O_2^{\bullet -}$, $HO_2^{\bullet}$. It is possible that photogenerated electrons can also reduce particulate Fe(III) to Fe(II), thereby promoting photoreductive dissolution of γ-Fe_2O_3. However, the lack of appreciable Fe(II) formation in irradiated γ-Fe_2O_3 systems either suggests photoassisted Fe(II) formation is not occurring, or that the Fe(II) generated *via* this process is rapidly oxidized in the near surface region, such that it cannot accumulate in bulk solution. For example, reactive oxygen species generated in the presence of light could oxidize Fe(II) to Fe(III).[20] This is proposed to be the main reason for the very high Fe(III) concentration (and limited soluble Fe(II)) observed with γ-Fe_2O_3 during irradiation experiments.

S(IV) oxidation in ATD systems

Absence of any measurable dissolved iron in the presence of ATD suggests that S(IV) oxidation in ATD suspensions is entirely heterogeneous in nature. We presume that Fe(II) generated in the surface-mediated oxidation of S(IV) on ATD particles is either unable to be released to the bulk aqueous solution or present at very low levels (*i.e.*, below the method detection limit) and thus unlikely to drive extensive S(IV) oxidation in homogeneous solution. Such limited dissolution might be expected if Fe(III) present in aluminosilicates were the primary oxidant, as generated Fe(II) would remain tightly bound in the aluminosilicate lattice after formation. Alternatively, Fe(II) generated from other iron phases (*e.g.*, oxides) may be rapidly oxidized and reprecipitated as Fe(III) on the ATD particle surface as a result of the pH increase we observed in ATD suspensions, thereby potentially inhibiting measurable iron dissolution. Finally, TiO_2 present in ATD or Ti leached into the aqueous phase from TiO_2 may also play a role in the very high rates for S(IV) oxidation observed in these experiment.[4,12] For example, previous studies by Harris *et al.* indicate that Ti is leached from mineral dust with an efficiency comparable to iron, and it can also participate in TMI catalyzed oxidation.[4,12] They also suggested that Ti/Fe synergistic effects can also play a role in TMI catalyzed oxidation.

Interestingly, there is no change in sulfur oxidation kinetics as a function of temperature or light for ATD. This result is in contrast to a recent chamber study that showed a factor of ten increase in the kinetic uptake coefficient on ATD in the presence of light.[26] These differences are unclear at this time but warrant further investigation. Further, there is a possibility for the formation of reactive oxygen species that enhance S(IV) oxidation under irradiation. However, it is likely that these reactions are much less significant in the presence of ATD due to the high pH (pH ~ 6) of the reaction mixture.

Conclusions and environmental implications

Collectively, these results demonstrate the complexity of sulfur oxidation on different mineral dust and other transition metal containing aerosol, especially iron-containing samples. In fact, to the best of our knowledge, this is the first study to show these very different effects of temperature and light in the presence of different iron-containing and other metal-containing aerosols. Most importantly, this study shows large differences in mechanisms that can occur for S(IV) oxidation depending on source and characteristics of particles and their transition metal ions. The effect of temperature and light on S(IV) oxidation to sulfate is quite different for FA, γ-Fe_2O_3 and ATD. Catalyzed S(IV) oxidation in the presence of mineral aerosol, at least partly, occurs *via* a heterogeneous pathway, especially at early stages of the reaction coordinate. Therefore, both particle phase as well as solution phase sulfate should be simultaneously quantified in order to accurately understand the S(IV) oxidation pathway. The temporal evolution of iron into the aqueous phase, Fe(III) as well as Fe(II), provides useful information about the S(IV) oxidation pathway. Concentration of dissolved iron is an important factor that determines the

 This journal is © The Royal Society of Chemistry 2016

Open Access Article. Published on 13 October 2016. Downloaded on 3/28/2024 8:14:22 PM.
This article is licensed under a Creative Commons Attribution 3.0 Unported Licence.



importance of TMI catalyzed oxidation pathway over other S(IV) oxidation mechanisms to form S(VI). In general, iron concentrations in atmospheric aqueous phase including cloud, fog and rain drops is in the μM range for a wide range of pH values ($2 \leq pH \geq 7$).[15] For example, in a field study by Pehkonen *et al.*, it was found that the concentration of Fe(II) and Fe(III) in cloud water varies from 0.3–0.5 μM and 0.6–1.4 μM, respectively.[27] In this study, the variation of Fe(II) and Fe(III) concentrations are 0–4 μM and 0–12 μM. Therefore the iron concentrations observed in the current study resemble real atmospheric concentration. These studies reported here are sorely needed for atmospheric models if they are to accurately predict sulfate formation, especially in severe winter haze conditions in China where current models under predict such values.

Acknowledgements

This material is based on the work supported by the National Science Foundation under grant number CHE-1639757. Any opinions, findings, and conclusions or recommendations expressed in this material are those of the authors and do not necessarily reflect the views of National Science Foundation.

References

1 H. M. Hung and M. R. Hoffmann, *Environ. Sci. Technol.*, 2015, **49**, 13768–13776.
2 E. Harris, B. R. Sinha, P. Hoppe and S. Ono, *Environ. Sci. Technol.*, 2013, **47**, 12174–12183.
3 C. Liu, Q. Ma, Y. Liu, J. Ma and H. He, *Phys. Chem. Chem. Phys.*, 2012, **14**, 1668–1676.
4 E. Harris, B. Sinha, S. Foley, J. Crowley, S. Borrmann and P. Hoppe, *Atmos. Chem. Phys.*, 2012, **12**, 4867–4884.
5 Y. Wang, Q. Zhang, J. Jiang, W. Zhou, B. Wang, K. He, F. Duan, Q. Zhang, S. Philip and Y. Xie, *J. Geophys. Res.: Atmos.*, 2014, **119**, 10425–10440.
6 X. Huang, Y. Song, C. Zhao, M. Li, T. Zhu, Q. Zhang and X. Zhang, *J. Geophys. Res.: Atmos.*, 2014, **119**, 14165–14179.
7 H. He, Y. Wang, Q. Ma, J. Ma, B. Chu, D. Ji, G. Tang, C. Liu, H. Zhang and J. Hao, *Sci. Rep.*, 2014, **4**, 4172.
8 B. Zheng, Q. Zhang, Y. Zhang, K. He, K. Wang, G. Zheng, F. Duan, Y. Ma and T. Kimoto, *Atmos. Chem. Phys.*, 2015, **15**, 2031–2049.
9 G. Zheng, F. Duan, H. Su, Y. Ma, Y. Cheng, B. Zheng, Q. Zhang, T. Huang, T. Kimoto and D. Chang, *Atmos. Chem. Phys.*, 2015, **15**, 2969–2983.
10 B. Ervens, *Chem. Rev.*, 2015, **115**, 4157–4198.
11 X. Zhang, Y. Wang, T. Niu, X. Zhang, S. Gong, Y. Zhang and J. Sun, *Atmos. Chem. Phys.*, 2012, **12**, 779–799.
12 E. Harris, B. Sinha, D. van Pinxteren, A. Tilgner, K. W. Fomba, J. Schneider, A. Roth, T. Gnauk, B. Fahlbusch and S. Mertes, *Science*, 2013, **340**, 727–730.
13 B. C. Faust, M. R. Hoffmann and D. W. Bahnemann, *J. Phys. Chem.*, 1989, **93**, 6371–6381.
14 B. Alexander, R. J. Park, D. J. Jacob and S. Gong, *J. Geophys. Res.: Atmos.*, 2009, **114**(D2), D02309.
15 L. Deguillaume, M. Leriche, K. Desboeufs, G. Mailhot, C. George and N. Chaumerliac, *Chem. Rev.*, 2005, **105**, 3388–3431.
16 D. M. Cwiertny, J. Baltrusaitis, G. J. Hunter, A. Laskin, M. M. Scherer and V. H. Grassian, *J. Geophys. Res.: Atmos.*, 2008, **113**, D05202.
17 H. Chen and V. H. Grassian, *Environ. Sci. Technol.*, 2013, **47**, 10312–10321.
18 H. Chen, A. Laskin, J. Baltrusaitis, C. A. Gorski, M. M. Scherer and V. H. Grassian, *Environ. Sci. Technol.*, 2012, **46**, 2112–2120.
19 R. E. Humphrey, M. H. Ward and W. Hinze, *Anal. Chem.*, 1970, **42**, 698–702.
20 H. Fu, D. M. Cwiertny, G. R. Carmichael, M. M. Scherer and V. H. Grassian, *J. Geophys. Res.: Atmos.*, 2010, **115**, D11304.
21 A. Rani, D. Prasad, P. Madnawat and K. Gupta, *Atmos. Environ.*, 1992, **26**, 667–673.
22 C. Brandt and R. Van Eldik, *Chem. Rev.*, 1995, **95**, 119–190.
23 B. C. Faust and M. R. Hoffmann, *Environ. Sci. Technol.*, 1986, **20**, 943–948.
24 X. Shen, T. Lee, J. Guo, X. Wang, P. Li, P. Xu, Y. Wang, Y. Ren, W. Wang, T. Wang, Y. Li, S. A. Carn and J. L. Collett Jr, *Atmos. Environ.*, 2012, **62**, 502–511.
25 H. Chen, C. E. Nanayakkara and V. H. Grassian, *Chem. Rev.*, 2012, **112**, 5919–5948.
26 J. Y. Park and M. Jang, *RSC Adv.*, 2016, **6**, 58617–58627.
27 S. O. Pehkonen, Y. Erel and M. R. Hoffmann, *Environ. Sci. Technol.*, 1992, **26**, 1731–1736.